Control of hearing sensitivity by tectorial membrane calcium

Clark Elliott Strimbu[a,1,2], Sonal Prasad[a,1], Pierre Hakizimana[a], and Anders Fridberger[a,3]

[a]Department of Clinical and Experimental Medicine, Division of Neurobiology, Linköping University, SE-581 83 Linköping, Sweden

Edited by Christine Petit, Institut Pasteur, College de France, INSERM, Université Pierre-et-Marie-Curie, Paris 15, France, and approved February 7, 2019 (received for review March 26, 2018)

When sound stimulates the stereocilia on the sensory cells in the hearing organ, Ca^{2+} ions flow through mechanically gated ion channels. This Ca^{2+} influx is thought to be important for ensuring that the mechanically gated channels operate within their most sensitive response region, setting the fraction of channels open at rest, and possibly for the continued maintenance of stereocilia. Since the extracellular Ca^{2+} concentration will affect the amount of Ca^{2+} entering during stimulation, it is important to determine the level of the ion close to the sensory cells. Using fluorescence imaging and fluorescence correlation spectroscopy, we measured the Ca^{2+} concentration near guinea pig stereocilia in situ. Surprisingly, we found that an acellular accessory structure close to the stereocilia, the tectorial membrane, had much higher Ca^{2+} than the surrounding fluid. Loud sounds depleted Ca^{2+} from the tectorial membrane, and Ca^{2+} manipulations had large effects on hair cell function. Hence, the tectorial membrane contributes to control of hearing sensitivity by influencing the ionic environment around the stereocilia.

hearing | temporary threshold shift | mechanoelectrical transduction | tectorial membrane | calcium

The sense of hearing depends on mechanically sensitive ion channels located near the tips of the stereocilia on the sensory hair cells of the inner ear (1). When an acoustic stimulus causes these mechanoelectric transduction (MET) channels to be activated, the flow of potassium and calcium ions into the cell increases (2).

The Ca^{2+} concentration ($[Ca^{2+}]$) in the vicinity of the MET channels is functionally important. For instance, it controls the fraction of MET channels that are open at rest [i.e., high calcium near stereocilia tends to close MET channels, whereas lower calcium does the opposite (3)]. Changes in the resting open probability alter the amplitude of the "silent current" (4, 5) that continuously flows into the sensory cells, causing them to operate at a relatively depolarized membrane potential near −40 mV (6). The continuous depolarization is important in one class of sensory cell, the outer hair cell, where it is thought to facilitate the detection of soft sounds by allowing amplification mediated by somatic electromotility (7) to operate at auditory frequencies (6).

Like other sensory receptors, hair cells possess an adaptation mechanism that reduces the transduction current in response to sustained stimuli (8). The conventional model states that this adaptation is due to two distinct processes, termed fast and slow adaptation, which operate on different time scales (9), but which both may depend on Ca^{2+} entry. In fast adaptation, or Ca^{2+}-mediated channel reclosure, Ca^{2+} ions appear to interact directly with the MET channel or its accessory proteins, causing the channel to rapidly close. Slow adaptation is believed to rely on the Ca^{2+}-dependent activation of unconventional myosins (10, 11), which move the upper insertion point of the tip links (12, 13), the tiny extracellular filaments that control the gating of the MET channels (14). By adjusting the tension in the tip links, slow adaptation reduces the MET current following prolonged deflections in the positive direction, thus ensuring that the MET channels maintain their responsiveness. Together, the two adaptation processes provide the hair cell with a high-pass filter and the dynamic range of the transduction apparatus is extended. Additionally, in both processes, as the MET channels close, they exert a pulling force on the tip links that leads to a measurable change in the position of the entire bundle of stereocilia (15, 16). This mechanical correlate of adaptation results in active hair bundle motility that may contribute to the amplification of faint sounds, a function that is critical for hearing (17). Much of the understanding of the two adaptation processes came from experiments performed on low-frequency hair cells from nonmammalian vertebrates. Despite the success of the model in explaining the observed MET currents in these low-frequency cells, recent work has questioned the extent to which this model of Ca^{2+}-dependent adaptation applies to mammalian hearing organs. Indeed, one recent report suggests that cochlear hair cell adaptation is, in fact, independent of Ca^{2+} entry (18), while others reached the opposite conclusion (19).

Due to its obvious physiological importance, significant effort was expended in measuring the level of Ca^{2+} in the fluid that surrounds stereocilia, the endolymph. These measurements, which were performed with ion-selective electrodes or by analyzing aspirated endolymph samples, showed values ranging from 15 to 40 μM (20–23). With the understanding that the results are controversial, cochlear hair cells from mice (19) and rats (18) tend to show little adaptation, and the number of MET channels open at rest increases substantially when stereocilia are exposed to solutions with micromolar $[Ca^{2+}]$.

Recent data suggest that the Ca^{2+} component of the receptor current may also be important for maintaining the structural

Significance

A new mechanism that contributes to control of hearing sensitivity is described here. We show that an accessory structure in the hearing organ, the tectorial membrane, affects the function of inner ear sensory cells by storing calcium ions. When the calcium store is depleted, by brief exposure to rock concert-level sounds or by the introduction of calcium chelators, the sound-evoked responses of the sensory cells decrease. Upon restoration of tectorial membrane calcium, sensory cell function returns. This previously unknown mechanism contributes to explaining the temporary numbness in the ear that follows from listening to sounds that are too loud, a phenomenon that most people experience at some point in their lives.

Author contributions: C.E.S. and A.F. designed research; C.E.S., S.P., and P.H. performed research; A.F. analyzed data; and A.F. wrote the paper.

The authors declare no conflict of interest

This article is a PNAS Direct Submission.

[1]C.E.S. and S.P. contributed equally to this work.

[2]Present address: Department of Otolaryngology, Columbia University Medical Center, New York, NY 10032.

[3]To whom correspondence should be addressed. Email: anders.fridberger@liu.se.

Published online March 5, 2019.

integrity of stereocilia. When isolated rat or mouse hair cells were exposed to MET channel blockers, the length of individual stereocilia and the architecture of the bundle were altered (24). These changes, which were reversible upon washout of the blocker, could also be induced by increasing the internal Ca^{2+} buffering capacity of the hair cells or by decreasing external Ca^{2+} to levels around 100 μM.

It seems clear that it is important to determine the $[Ca^{2+}]$ close to the hair bundles, particularly since a previous study (25) suggested that local Ca^{2+} may be elevated as a result of high activity of plasma-membrane calcium-ATPase type 2, coupled with diffusion barriers imposed by the proximity to the tectorial membrane, an acellular accessory structure close to stereocilia. However, all reported measurements of $[Ca^{2+}]$ in the inner ear fluids used techniques that lack spatial resolution, so the Ca^{2+} level near the stereocilia is not known.

Here, we used fluorescence imaging and spectroscopic measurements to determine Ca^{2+} in situ. Surprisingly, these experiments revealed that the tectorial membrane had a much higher Ca^{2+} concentration than the surrounding endolymph, and that reductions in tectorial membrane Ca^{2+} contributed to the acute decrease of hearing sensitivity experienced immediately after loud sound exposure.

Results

To measure $[Ca^{2+}]$ near the hearing organ, we used temporal bone preparations isolated from guinea pigs (26). The preparations retained the middle ear, allowing sound stimulation through a loudspeaker positioned in the ear canal, and to ensure cellular viability, the preparations were continuously perfused with oxygenated tissue culture medium. A small opening at the apex of the cochlea allowed a glass microelectrode with 10-μm tip diameter to be positioned close to the hearing organ. The electrode was used to introduce the low-affinity fluorescent indicator Asante Calcium Red. When excited at 488 nm, this dye emitted red light with intensity that depended on the Ca^{2+} level, as well as green light with very weak Ca^{2+} dependence (27). By taking the ratio between red and green fluorescence intensities, spatial and temporal variations in dye concentration were cancelled out and a sensitive measure of extracellular $[Ca^{2+}]$ was obtained.

High Ca^{2+} Within the Tectorial Membrane. A pivotal finding from these experiments was that Ca^{2+} levels were much higher in the tectorial membrane than in the surrounding fluid. This pattern was evident in single images (Fig. 1*A*), where high ratios were evident in tectorial membrane regions close to the hair cells, as well as in the region close to the attachment to the spiral limbus.

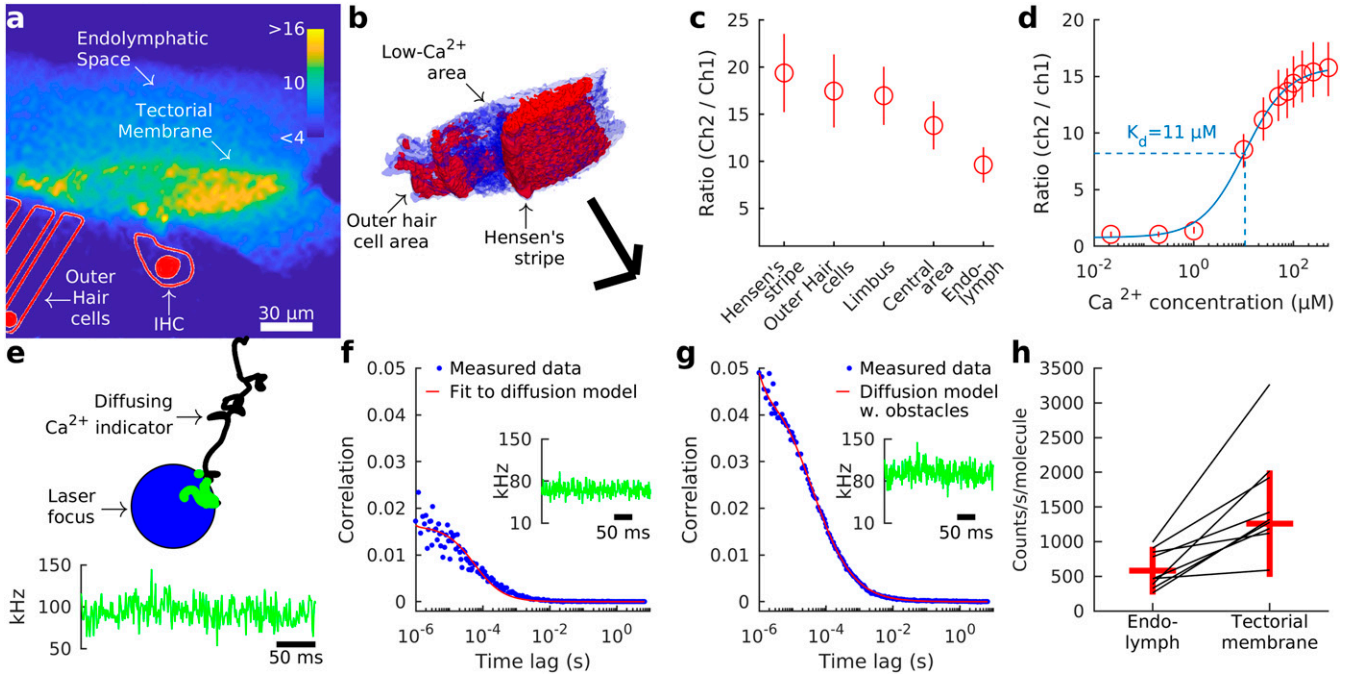

Fig. 1. High tectorial membrane Ca^{2+}. (*A*) Following injection of the low-affinity ratiometric Ca^{2+} dye Asante Calcium Red into the endolymphatic space, high Ca^{2+} levels were evident in the tectorial membrane. The locations of the outer and inner hair cells are indicated by the red lines. IHC, inner hair cell. (*B*) Three-dimensional reconstruction made from 100 confocal images acquired with 1-μm section spacing. The red color denotes voxels with a Ca^{2+} ratio >18; regions with a ratio between 15 and 18 are colored blue. (Scale bars: 50 μm for the *X*, *Y*, and *Z* planes.) (*C*) Average Ca^{2+} ratios in different regions of the tectorial membrane ± 1 SD across 27 different preparations. Ch, channel. (*D*) Asante Calcium Red was dissolved in artificial endolymph with varying $[Ca^{2+}]$ and imaged with settings identical to those used in *C*. The blue line is a fit to the Hill equation, with $n = 1$. Values of the mean ± 1 SD from five images at each calcium concentration are illustrated. Fit parameters: $R_{max} = 16$, $R_{min} = 0.7$, $K_d = 11$ μM. (*E*) Principle of fluorescence correlation spectroscopy. Ca^{2+} indicator molecules that enter the focus of a laser beam will be excited and emit green light. The emitted light, which passes a pinhole that blocks out-of-focus light, is detected by a photon-counting detector. As molecules randomly enter and leave the detection volume, the photon count at the detector rapidly fluctuates, as shown in the graph (the *y* axis shows the count rate in kilohertz). (*F*) Example of fluorescence fluctuations recorded after injecting Oregon Green 488 BAPTA-5N in the endolymphatic fluid space (*Inset*) and their autocorrelation function (blue dots in main diagram). A function describing 3D diffusion was fitted to the correlation data (red line). The average number of molecules in the detection volume is equal to 1 divided by the *y*-axis intercept of the fitted curve. The molecular brightness is determined by dividing the average count rate by the number of molecules. (*G*) Correlation curve acquired with the laser focus positioned inside the tectorial membrane (blue dots). The red line is a fit to a model describing confined diffusion. Data are from the same preparation as in *F*. The higher amplitude of the curve (compared with *F*) is caused by a smaller number of molecules in the detection volume. The diffusion time is 40 μs. (*H*) Molecular brightness in the endolymph and in the tectorial membrane. Horizontal red lines show the mean values, and vertical red lines indicate ±1 SD. Thin black lines connect endolymph data with the tectorial membrane data from each of nine preparations. Identical acquisition settings were used in all nine experiments, and multiple correlation curves were acquired in each experiment.

The pattern was also evident in 3D reconstructions made from confocal images acquired at 1- to 5-μm intervals (Fig. 1*B*; the red color corresponds to regions with a fluorescence ratio >18, and regions with a smaller ratio are colored blue). The highest fluorescence ratio (Fig. 1*C*; 19.4 ± 4.2, mean ± SD; $n = 27$ experiments) was found in a region of the tectorial membrane close to the stereocilia of the inner hair cells (Hensen's stripe in Fig. 1*B*). High Ca^{2+} ratios were also found near the outer hair cells (17.5 ± 3.9) and near the spiral limbus (16.9 ± 3.1), whereas smaller values were evident in the bulk of the endolymphatic fluid (9.6 ± 1.9) and in the central region of the tectorial membrane (13.8 ± 2.6; the central region is the low-Ca^{2+} area shown in Fig. 1*B*). These regional differences were statistically significant ($P < 2 \times 10^{-16}$, repeated-measures analysis of variance; $F = 239$; post hoc analysis using t tests with Bonferroni corrections showed that all regions within the tectorial membrane were significantly different from the endolymph, $P < 1 \times 10^{-15}$ for all comparisons).

To convert these fluorescence ratios to absolute [Ca^{2+}], we imaged dye molecules dissolved in artificial endolymph with varying [Ca^{2+}]. Fits of the fluorescence ratios to the Hill equation (Fig. 1*D*) gave a dissociation constant of 11 μM, close to the manufacturer's estimate, which suggested an average endolymphatic [Ca^{2+}] near 15 μM, a value consistent with previous measurements (15–40 μM) (20–23). However, in these calibrations, we could not achieve Ca^{2+} ratios as high as the ones observed in regions of the tectorial membrane near hair cell stereocilia. It is formally possible that the dye reacted with components of the tectorial membrane, leading to artificially elevated fluorescence ratios. Furthermore, Asante Calcium Red's weak fluorescence necessitated the use of relatively high dye concentrations, which may cause buffering effects. Such buffering effects can distort spatial and temporal variations in Ca^{2+} (28) and result in difficulties in estimating the Ca^{2+} level of the tectorial membrane.

To exclude buffering effects and chemical binding of the indicator to the tectorial membrane, the above results were verified using injections of nanomolar concentrations of the low-affinity Ca^{2+} indicator Oregon Green 488 BAPTA-5N and a measurement technique, fluorescence correlation spectroscopy (29, 30), which works at such low indicator concentrations. In brief, a laser beam was focused to a submicron spot close to the hearing organ (schematic in Fig. 1*E*). As the indicator molecules randomly entered and departed the detection volume, rapid fluorescence fluctuations occurred, as seen in the graph in Fig. 1*E*. This trace contained information about the number of molecules present in the laser focus, their residence time, and their molecular brightness, all of which were accessed by computing the autocorrelation of the fluorescence fluctuations (30). In the example data shown in Fig. 1*F*, recorded in the endolymph, a model describing the 3D diffusion of indicator molecules (red line) was fitted to the measured correlation curve (blue dots). The fit parameters revealed that an average of 61 molecules were present in the laser focus and that their mean residence time was 55 μs.

Moving the laser focus inside the tectorial membrane (Fig. 1*G*) changed the correlation curve, and the standard diffusion model no longer fitted the data because of excessive amplitudes at lag times between 0.1 and 1 ms. Such correlation curves are expected when fluorescent molecules diffuse through a fluid space crowded with macromolecules, and a model of hindered 3D diffusion (31) hence provided an excellent fit (red line in Fig. 1*G*). Since moving molecules are the only ones that generate correlation curves like the ones in Fig. 1 *F* and *G*, these data demonstrate that the indicator was not bound to the tectorial membrane. Typically, fewer indicator molecules were present in recordings from the tectorial membrane (e.g., 21 in Fig. 1*G* vs. 61 in Fig. 1*F*), but fluorescence rates were nevertheless higher (Fig. 1*G*, *Inset* vs. Fig. 1*F*, *Inset*). Evidently, indicator molecules residing within the tectorial membrane had higher brightness per molecule than those in the endolymph. Since the fluorescence intensity of the dye depends on Ca^{2+}, this shows that the Ca^{2+} level in the tectorial membrane is higher than that of the endolymph (Fig. 1*H*; $P = 0.002$ by paired t test, with 8 df based on 33 averaged correlation curves from the endolymph and 46 inside the tectorial membrane; $n = 9$ individual preparations).

Since both ratiometric Ca^{2+} imaging and fluorescence correlation spectroscopy showed the same pattern, we conclude that [Ca^{2+}] is higher within the tectorial membrane than the surrounding endolymph.

Loud Sounds Depleted Tectorial Membrane Ca^{2+}. To determine whether tectorial membrane Ca^{2+} was regulated, preparations were exposed to loud sound at levels similar to those found at rock concerts. Ratio images before overstimulation (Fig. 2*A*) again demonstrated high [Ca^{2+}] near sensory cell stereocilia, but a substantial decrease occurred after exposure to 10 min of loud sound at 98 dB sound pressure level (SPL) and 140 Hz, a frequency slightly below the best frequency of the recording location (Fig. 2*B*). On average (Fig. 2*C*), the Ca^{2+} ratio at Hensen's stripe changed from 22.5 ± 13 to 12.8 ± 10.1 ($P = 0.0002$ by paired t test with Bonferroni corrections, df = 15, $t = 5.65$; $n =$ 16 preparations). Significant decreases were also observed for other regions within the tectorial membrane, as well as in the endolymph (the endolymph changed from a ratio of 12 ± 7 to 8.7 ± 6.4; $P = 0.02$ by paired t test with Bonferroni corrections, $t = 3.28$; $n = 16$ preparations).

The electrode that introduced Ca^{2+} indicators in the endolymph was also used to record the electrical potentials that hair cells produced in response to acoustic stimulation at 64 dB SPL. By tracking the amplitude of these microphonic potentials while sweeping the sound stimulus frequency, tuning curves were acquired. In the preparation shown in Fig. 2*D*, loud sound decreased the microphonic amplitude by more than 20 dB in the region near the peak, while smaller changes were observed at higher stimulus frequencies. To examine the relation of these changes to tectorial membrane Ca^{2+}, images and electrophysiological data were acquired at ∼5-min intervals.

The red solid line in the top half of Fig. 2*E* plots the peak amplitude of the microphonic potential over time in an example preparation. Note the decreased amplitude immediately after loud sound exposure and the gradual recovery that took place thereafter (partial recovery of microphonic potentials was observed in eight of 16 preparations). The Ca^{2+} ratio (red solid line in Fig. 2*E*, *Bottom*) also decreased, and showed recovery over the same time scale as the electrical potentials. Data from a different preparation (green solid lines in Fig. 2*E*) illustrate a second pattern. Despite identical sound exposure parameters, this preparation showed no significant recovery from overstimulation, neither in electrical potentials nor in Ca^{2+}. These data suggested a correlation between tectorial membrane Ca^{2+} and sound-evoked electrical potentials. Over the entire dataset of 16 preparations, significant correlations were indeed found between the microphonic potentials and Ca^{2+} in the outer hair cell region (average $r = 0.71$, range 0.23–0.99; $P = 0.01$ by t test with Bonferroni corrections for multiple comparisons, $t = 3.79$) and with Ca^{2+} in Hensen's stripe ($r = 0.64$, $P = 0.035$), but not with the central region of the tectorial membrane ($r = 0.61$, $P = 0.06$) or the endolymph ($r = 0.47$, $P = 0.33$). This finding suggested that changes in tectorial membrane Ca^{2+} were an important contributor to the acutely decreased hearing sensitivity observed after brief loud sound exposure.

Loud sounds cause complex changes, which may include gross disruption of hearing organ morphology, destruction of tip links, and alterations in sound-evoked stereocilia motion (reviewed in ref. 32). However, apart from minor, inconsistent changes in the intensity of staining, loud sound at the levels and durations used in these experiments caused no observable change in stereocilia morphology (Fig. 2*F*). The area of the tectorial membrane showed

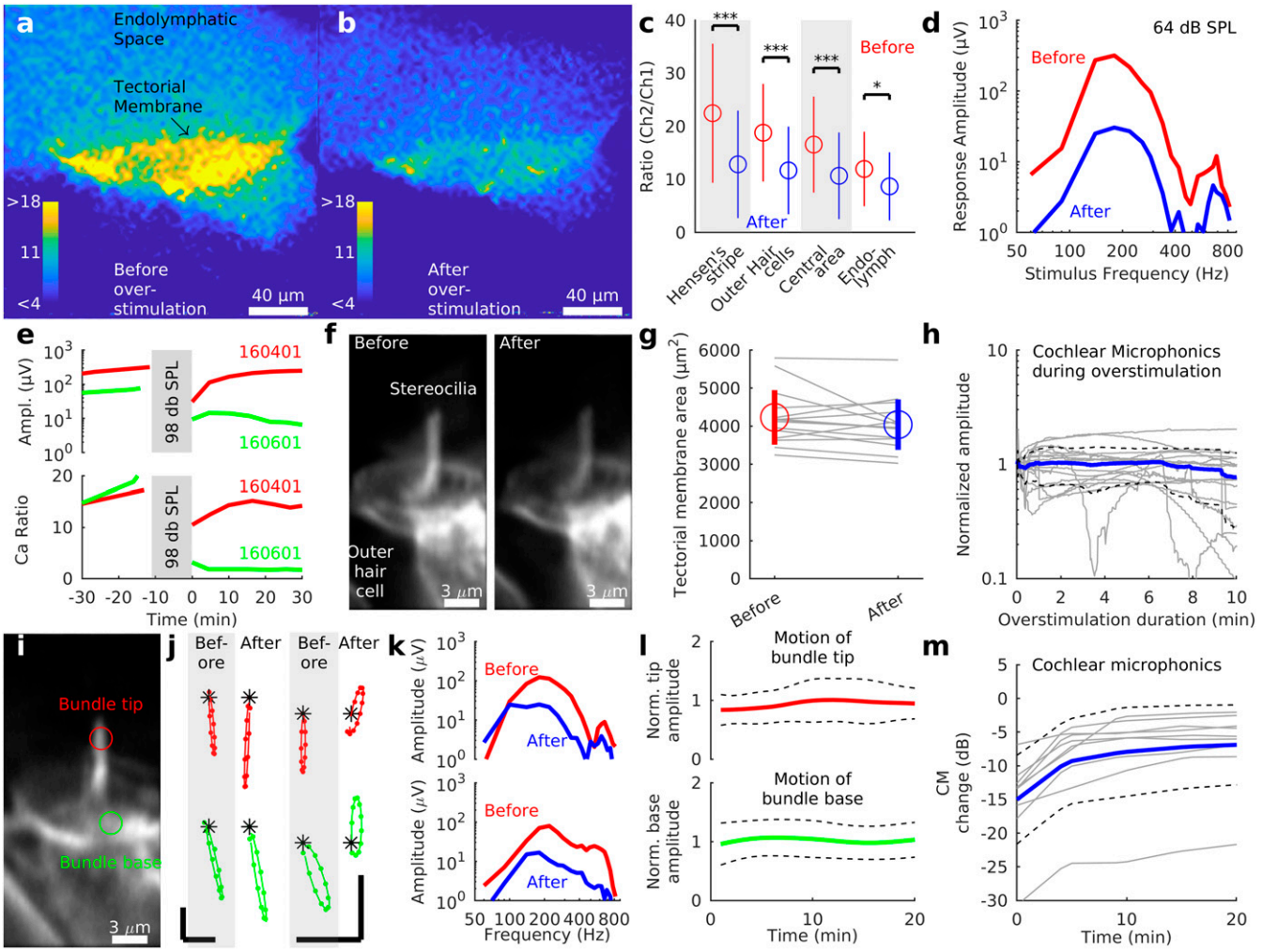

Fig. 2. Loud sounds depleted tectorial membrane Ca^{2+}. Ca^{2+} ratio images before (*A*) and after (*B*) 10 min of acoustic overstimulation at 140 Hz and 98 dB SPL. (*C*) Mean ± SD of Ca^{2+} ratio changes across 16 preparations. Ch, channel. Red data are before overstimulation, and blue data are afterward. Exposure parameters are as in *A*. $*P < 0.05$; $***P < 0.001$. (*D*) Tuning curves for the cochlear microphonic potential before and after overstimulation in an example preparation. (*E*, *Top*) Peak amplitude of the cochlear microphonic potential over time in two example preparations. (*E*, *Bottom*) Tectorial membrane Ca^{2+} ratio over time in the same preparations. Note the correspondence between Ca^{2+} changes and the amplitude of the cochlear microphonic potential in each preparation. (*F*) Apart from minor brightness changes, overstimulation had no effect on the morphology of outer hair cell stereocilia. (*G*) Tectorial membrane areas before and after overstimulation. Thin gray lines show data from individual preparations, vertical blue and red lines depict ±1 SD, and the rings show the means. (*H*) Normalized peak amplitude of the cochlear microphonic potential during overstimulation. The thick blue line denotes the mean, and dashed lines indicate ±1 SD. Thin solid lines show data from individual preparations. (*I*) Outer hair cell stereocilia imaged by time-resolved confocal microscopy during sound stimulation at 180 Hz and 64 dB SPL. (*J*) Motion of the bundle tip (red) and base (green) before and after overstimulation. Asterisks denote the starting point of each motion trajectory. One set of trajectories are from one example preparation (*Left*), and another set of trajectories are from another preparation (*Right*). (Scale bars: 100 nm.) (*K*) Cochlear microphonic potential tuning curves from the preparations shown in *J*. (*L*) Averaged motion at the tip of outer hair cell stereocilia (*Top*, red line) and at their base (*Bottom*, green line) after overstimulation. Data were normalized to the average trajectory amplitude recorded before overstimulation. Broken lines indicate 1 SD. (*M*) Despite the lack of change in stereocilia motion, as shown in *L*, the amplitude of the cochlear microphonic potential decreased by 14 ± 7 dB at its peak. The sound stimulus level was 64 dB SPL. Thin gray lines show data from individual preparations, the thick blue line denotes the mean, and dashed lines denotes the SD. CM, cochlear microphonic potential.

no significant change (Fig. 2*G*; 4,230 ± 718 μm^2 before overstimulation vs. 4,040 ± 663 μm^2 after overstimulation; $P = 0.15$, df = 14, $t = 1.5$ by paired t test; in two of 15 cases, there was no area change, whereas five preparations had an increasing area and eight showed a decrease).

If the loud sounds had rendered the MET channels nonfunctional, channel activation would be impossible at any sound pressure, and we therefore tracked the amplitude of sound-evoked electrical potentials during the progression of the loud sound exposure. The microphonic potentials, however, decreased by less than 3 dB during 10 min of loud sound, despite a 14 ± 7 dB average reduction in responses to sound at lower levels (Fig. 2*H*). This small change suggests that most MET channels were still functional, since these channels were apparently producing microphonic potentials with nearly constant amplitude throughout the duration of the loud sound exposure.

To determine whether loud sounds altered the input to the sensory cell stereocilia or their mechanical properties, sound-evoked hair bundle motions were measured by time-resolved confocal microscopy and optical flow (33) in a separate set of 10 experiments. Loud sound did change the sound-evoked motion of outer hair cell stereocilia, but these changes lacked consistency, as seen in Fig. 2 *I* and *J*. In the left set of trajectories in Fig. 2*J*, loud sound increased the displacement both at the tip of the stereocilia (red trajectory) and at its base (green trajectory), and led to small changes in the inclination of the major axis

of the trajectories. Despite the increased stereocilia motion, electrical potentials decreased (Fig. 2*K*, *Top*). In the right set of trajectories in Fig. 2*J*, acquired from a different preparation, overstimulation decreased sound-evoked motion and changed the phase of the response. The sound-evoked electrical potentials also decreased (Fig. 2*K*, *Bottom*).

Since loud sound increased sound-evoked stereocilia displacements slightly in some preparations and slightly decreased them in others, there was no average change in the sound-evoked motion measured at the base of stereocilia (Fig. 2*L*, *Bottom*; mean ± 1 SD, $n = 10$ preparations) or at their tip (Fig. 2*L*, *Top*). Sound-evoked electrical potentials, however, showed a 14 ± 7-dB decrease immediately after overstimulation (Fig. 2*M*), followed by partial recovery over the ensuing 20 min.

In summary, following these relatively mild loud sound exposures, similar to that experienced by many people at rock concerts, there was a significant decrease in the [Ca^{2+}] of the tectorial membrane. These Ca^{2+} changes correlated with the amplitude changes in the cochlear microphonic potential, but not with any other physiological parameter, suggesting that such Ca^{2+} changes influenced hearing sensitivity.

Is Tectorial Membrane Ca^{2+} a Control Parameter? To learn more about the role of Ca^{2+} for sound-evoked responses, we imaged Ca^{2+} changes with Asante Calcium Red before and after injecting the Ca^{2+} chelator EGTA directly into the endolymph. Since previous reports (34–36) showed that the tectorial membrane swells when exposed to solutions with low [Ca^{2+}], we injected solutions with only a small amount of EGTA (100 μM) dissolved in endolymph with 20 μM Ca^{2+}. This produced no change of tectorial membrane area in one preparation (compare Fig. 3*A* with Fig. 3*B*), a decreased area in one preparation, and swelling in three preparations (area before EGTA: 4,277 ± 443 μm^2; area after EGTA: 4,433 ± 413 μm^2; $n = 5$; $P = 0.14$, $t = -1.81$, df = 4 by paired t test). The Ca^{2+} ratio of the tectorial membrane dropped, but not to the level of the endolymph, since the tectorial membrane could still be distinguished from the surrounding fluid. In the preparation shown in Fig. 3 *A* and *B*, 35 min of recovery somewhat increased fluorescence ratios in the region close to the outer hair cells (Fig. 3*C*), but the ratios remained depressed elsewhere. Fig. 3*D* shows microphonic potential tuning curves from this preparation. Immediately after the EGTA injection, their amplitude decreased by 8 dB. The minor recovery of tectorial membrane Ca^{2+} seen in Fig. 3*C* was accompanied by a minor 2-dB increase in the microphonic potential.

Since the tips of the tallest stereocilia of the outer hair cells are embedded in the tectorial membrane (37), alterations in tectorial membrane mechanics will alter the sound-evoked motion of stereocilia, which would change the amplitude of the cochlear microphonic potential. To assess a possible contribution from subtle changes in the mechanical properties of the tectorial membrane or in stereocilia, we imaged sound-evoked hair bundle motion before and after EGTA injection.

The injection caused no morphological change in outer hair cell stereocilia (apart from minor inconsistent changes in brightness; Fig. 3 *E*–*G*). As seen in Fig. 3*H*, motion trajectories recorded from the tips of stereocilia (red) had an elongated elliptical shape that remained similar before and immediately after EGTA injection, and following 30 min of recovery. Trajectories from the base of stereocilia (green in Fig. 3*H*) had a larger amplitude than the tip trajectories, as previously described (38). After the EGTA injection, there was a minor change in the inclination of the trajectory, the shape of which became slightly more elliptical with time. Despite the lack of change in stereocilia morphology or sound-evoked motion, EGTA caused a substantial and mostly irreversible decline of the cochlear microphonic potential (Fig. 3*I*; −6.5 dB at the best frequency, 180 Hz; partial recovery was observed in two of 10 experiments).

Fig. 3*J* shows the change in sound-evoked motion at the base of the hair bundle across 10 preparations. EGTA caused a large decrease of motion in one experiment but no change in the remaining nine; thus, on average, there was no alteration in the motion of either the base (Fig. 3*J*) or the tip (Fig. 3*K*). By computing the difference between trajectories recorded from the tip and the base of stereocilia, a measure of bundle deflection is obtained. Consistent with previous reports (39), the deflection amplitude was slightly less than half of the base motion (Fig. 3*L*); no change was apparent after EGTA. Despite the lack of change in sound-evoked motions, the amplitude of the cochlear microphonic potential decreased by 9.2 ± 5 dB after EGTA (Fig. 3*M*), a significant difference from the control injections, which caused a 0.44 ± 1.78-dB decrease in the cochlear microphonic amplitude ($P = 3.4 \times 10^{-6}$, $t = 6.9$, df = 16; $n = 13$ controls).

The EGTA-induced decrease of the microphonic potential may have several different causes. Because the sound-evoked motion of stereocilia was not altered, changes in the passive mechanical properties of the hearing organ are unlikely. However, low Ca^{2+} may cause tip links to break (40). In this case, EGTA-induced changes in microphonic amplitudes are expected to be irreversible over the time scale of these experiments, since tip link regeneration is a slow process (41, 42).

To examine the reversibility of EGTA-induced changes, we performed experiments where EGTA was followed by injection of endolymph containing 1 mM Ca^{2+} (Fig. 4; $n = 7$ preparations). As shown in Fig. 4*A*, EGTA decreased the amplitude of the cochlear microphonic potential (compare center and top waveforms in Fig. 4*A*; the stimulus was a 64-dB SPL tone at the best frequency of the recording location, 140 Hz). Upon injection of high-Ca^{2+} endolymph, the microphonic potential showed substantial, but not complete, recovery (Fig. 4*A*, *Bottom*). This recovery was frequency-dependent. At frequencies below the peak of the tuning curve (Fig. 4*B*), Ca^{2+} caused the microphonic amplitude to increase above the control level in six of seven preparations. At the peak, the amplitudes of the tuning curve decreased by 5.3 ± 3.3 dB after EGTA (Fig. 4*C*), and a 3.5-dB average increase was observed after injection of high-Ca^{2+} endolymph. This increase was statistically significant ($P = 0.022$ by paired t test, 6 df, $t = -3.07$). At frequencies more than one octave above the peak, little recovery was seen.

Discussion

This study shows that the [Ca^{2+}] is higher within the tectorial membrane than in the surrounding endolymphatic fluid. We have also shown that loud sound depletes Ca^{2+} from the tectorial membrane, a change that is associated with an acute decrease of auditory sensitivity.

Several mechanisms may contribute to elevating Ca^{2+} within the tectorial membrane. Among them is the epithelial Ca^{2+} transport system (43, 44) and the plasma-membrane Ca^{2+}-ATPases, subtypes of which are present in hair cells, the stria vascularis, and the interdental cells of the spiral limbus (21). These pumps continuously move Ca^{2+} into the endolymph (25, 45). Furthermore, two of the most abundant proteins in the tectorial membrane, otogelin and alpha-tectorin, contain von Willebrand factor type D repeats (46), which can bind Ca^{2+} (47). Alpha-tectorin has sequence homology with entactin (48), a protein with Ca^{2+}-binding sites (49), and a close relative of alpha-tectorin binds Ca^{2+} in the urinary tract (50). Furthermore, at physiological pH, the tectorial membrane is negatively charged (51), which would have an attractive effect on positively charged ions. Based on these data, we propose that secretion of Ca^{2+} into the endolymph acts in concert with positive charges to elevate Ca^{2+} within the tectorial membrane, where binding sites may stabilize the [Ca^{2+}] by acting as a fixed buffer. The tectorial membrane may also restrict diffusion around the stereocilia, further elevating Ca^{2+} near the MET channels (25).

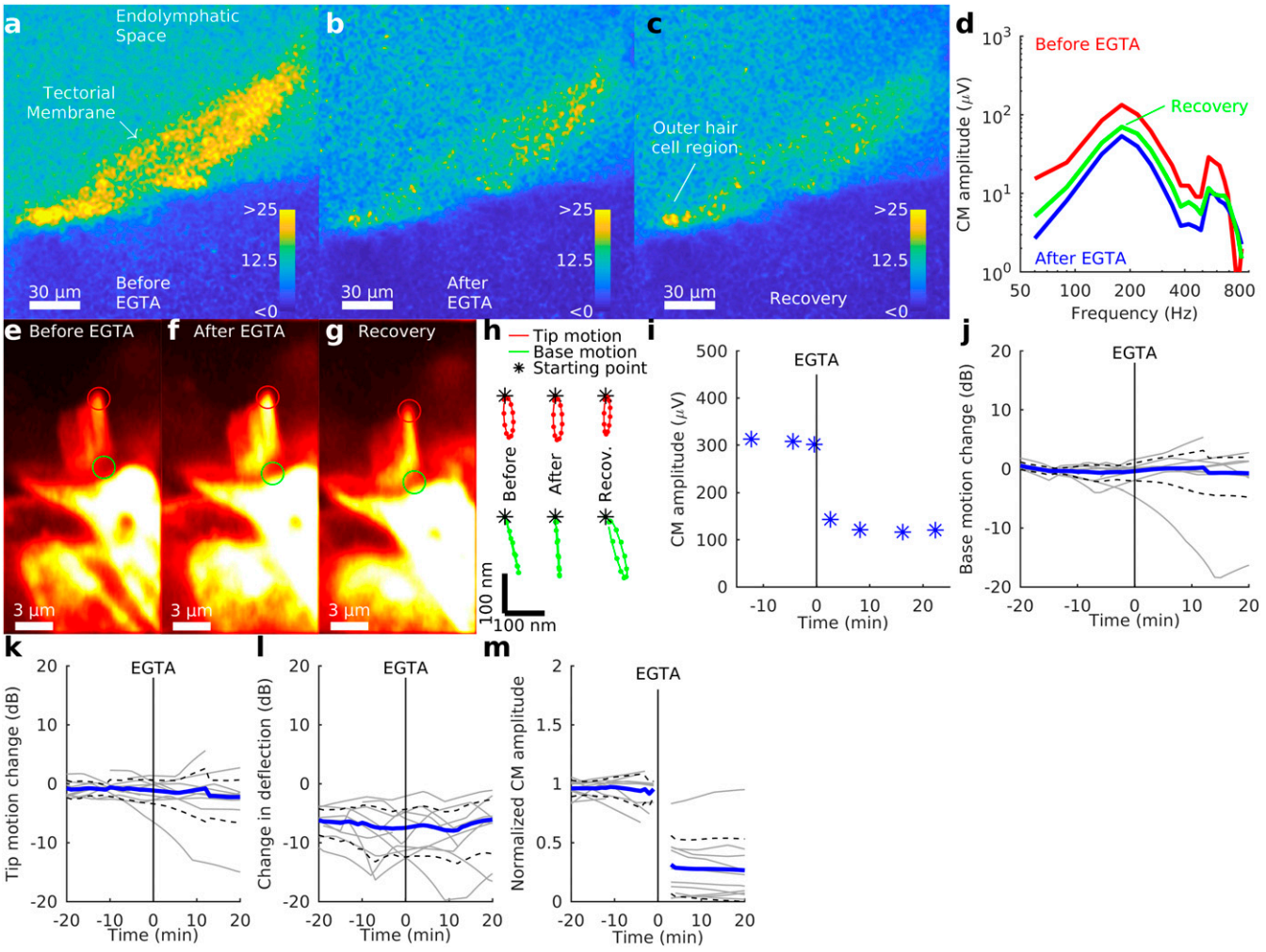

Fig. 3. Ca^{2+} chelators decrease the amplitude of the cochlear microphonic potential without affecting the sound-evoked motion of the cochlear partition. (*A–C*) Ca^{2+} ratio before, immediately after, and 35 min after EGTA injection in the scala media. (*D*) Cochlear microphonic potential tuning curves at 64 dB SPL at the times corresponding to the images in *A–C*. Note the decrease after EGTA injection, and partial recovery. CM, cochlear microphonic potential. (*E–G*) EGTA in the scala media had no effect on stereocilia morphology, except for a small change in the brightness of the fluorescent dye. These brightness changes lacked consistency across preparations. (*H*) Sound-evoked motion of the stereocilia tips (red) and their bases (green) in the preparations shown in *E–G*. Asterisks denote the starting point of each trajectory. (*I*) Peak amplitude of the cochlear microphonic potential in the experiment shown in *H*. The vertical line at time 0 indicates the time of injection of EGTA. (*J*) Change in sound-evoked motion at the base of outer hair cell stereocilia (blue line) ± 1 SD (dashed black lines). Thin gray lines show data from individual preparations. Data are from 10 individual preparations. (*K*) Normalized average motion of outer hair cell bundle tips before and after EGTA. Line types are as in *J*. (*L*) By subtracting trajectories from the tips and bases of stereocilia, a measure of the deflection of the bundle is obtained. Line types are as in *J* and *L*. (*M*) Despite the lack of change in stereocilia morphology or motion shown in *E* through *L*, the peak amplitude of the cochlear microphonic potential decreased substantially after EGTA injection. Line types are as in *J–L*.

The exact $[Ca^{2+}]$ within the tectorial membrane is difficult to pinpoint, since more precise measurements would require calibration of the Ca^{2+}-sensitive dyes in an environment precisely matching the one in the tectorial membrane, which is not technically feasible. However, in an endolymph-like solution, complete saturation of Asante Calcium Red is observed near 300 µM. It also seems likely that Ca^{2+} in the subtectorial space is elevated compared with the endolymph, but the magnitude is difficult to quantify because accurate delineation of the subtectorial space requires the use of dyes with emission spectra that overlap with commonly used indicator substances. Since the tip of the stereocilia are close to the tectorial membrane, the MET channels are likely exposed to higher calcium levels than previously thought. The bulk of presently available evidence suggests that this would increase adaptation, while reducing the resting open probability of MET channels (18, 19, 52).

When injections of EGTA were used to decrease the endolymphatic Ca^{2+} level, we observed changes in the amplitude of the microphonic potentials (Figs. 3 and 4) that were partially reversible upon injection of endolymph with 1 mM Ca^{2+}. The EGTA-induced decrease of microphonic potentials may occur through several mechanisms. First, although changes in tectorial membrane morphology were not apparent and the sound-evoked motions of the organ of Corti remained unchanged (Fig. 3), it is likely that Ca^{2+} changes larger than the ones seen here will alter the mechanical properties of the tectorial membrane (34–36), leading to an altered stimulation of sensory cell stereocilia. Second, while attempts to measure the resting open probability of the MET channels in vivo gave conflicting results (cf. ref. 53 and ref. 54, also the variability apparent in ref. 55), it is conceivable that changes in external $[Ca^{2+}]$ alter the fraction of MET channels that are open in silence. This could also affect the amplitude of the sound-evoked response. Finally, a decrease in

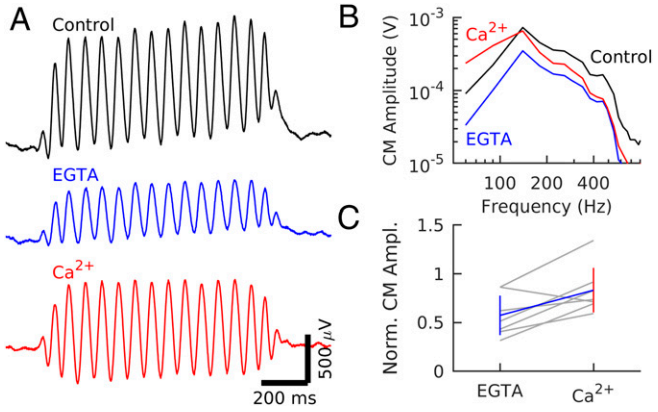

Fig. 4. Ca^{2+} partially reverses EGTA-induced changes. (*A*) Waveforms of the cochlear microphonic potential before EGTA (control, *Top*), after injection of 100 μM EGTA dissolved in normal endolymph (*Middle*), and after injection of endolymph with 1 mM Ca^{2+} (*Bottom*). The stimulus was a 140-Hz tone burst at 64 dB SPL. Each record represents the mean of 10 stimulus presentations. (*B*) Tuning curves of the cochlear microphonic potential (CM) at 64 dB SPL. Each curve was recorded by stepping the stimulus frequency from 60 to 800 Hz, with 10 averages at each frequency (different experiment than *A*). (*C*) Peak amplitudes were normalized to the amplitude before EGTA across seven preparations after EGTA and after Ca^{2+}. Thin gray lines show data from individual preparations, the blue line connects the means before and after, and vertical lines depict ±1 SD.

external Ca^{2+} can break the tip links responsible for MET channel gating (40), leading to receptor current changes not reversible over the time frame used in the present study. Since we were unable to completely reverse the EGTA effect by injecting Ca^{2+} (Fig. 4), a contribution from tip-link breakage is possible. These are findings with substantial pathophysiological importance, because loud sound decreased tectorial membrane Ca^{2+} (Fig. 2) in much the same way as EGTA, while Ca^{2+} increases in the sensory hair cells (56, 57).

At some point in life, most people experience the acute numbness in the ear that follows from listening to sounds that are excessively loud. The mechanisms producing this acutely decreased hearing sensitivity depend on the duration of the sound exposure and its pressure level. For instance, a 30-min exposure to continuous octave-band noise at 85 dB SPL caused a temporary hearing loss associated with activation of P2X2 receptors (58), whereas a 2-h, 100-dB SPL exposure to the same octave band of noise resulted in synaptic pathology (59). Because the presently used sound exposure, pure tones at 98 dB repeated every second during 10 min, must be considered very mild, changes in tectorial membrane Ca^{2+} are a previously unknown early mechanism of such temporary threshold shifts. As mentioned above, large Ca^{2+} changes may alter the mechanical properties of the tectorial membrane, move the operating point of the MET channels, and contribute to breakage of tip links. Tip links, however, may regenerate (41, 42), which would permit the gradual recovery of hearing.

The tectorial membrane is usually assumed to have a mechanical role (60–65), with its direct connection to the stereocilia of the outer hair cells and its influence on fluid flow around inner hair cells ensuring effective sensory cell stimulation. This mechanical role is supported by experiments in knockout mice, which revealed profound effects from structural disruptions of the tectorial membrane (54, 66). The present results suggest that these mutations also could change tectorial membrane Ca^{2+}, which may force some previous results to be reevaluated. For instance, otoancorin mutant mice (67) have tectorial membranes that lack Hensen's stripe, a structure with particularly high Ca^{2+} located close to the inner hair cell bundles (Fig. 1*A*). These animals have normal sound-evoked basilar membrane displacements but elevated neural thresholds (67), suggesting decreased inner hair cell sensitivity. Point mutations in the alpha-tectorin gene also disturb Hensen's stripe, and auditory brainstem responses are elevated relative to wild-type mice (68, 69). The present results raise the intriguing possibility that these mutants, in addition to the mechanical changes caused by disrupting the tectorial membrane, have inner hair cell bundles that lack sufficient Ca^{2+} for normal transduction.

Materials and Methods

Experimental Model and Subject Details. Before performing experiments, all protocols were approved by the Regional Ethics Board in Linköping, Sweden (Permit N32/13). Young mature (250–450 g) Dunkin–Hartley guinea pigs of either sex were anesthetized with 600–800 μL of 50 mg/mL sodium pentobarbital and decapitated. The temporal bones were excised and mounted in a custom-built chamber, and the bony wall of the bulla was gently removed with bone scissors. The entire preparation was immersed in oxygenated (95% O_2, 5% CO_2) cell culture medium (minimum essential medium with Earle's balanced salts) and maintained at room temperature (22–24 °C). A fine scalpel was used to cut a small triangular-to-trapezoidal opening of ~0.65 mm on each side, near the apex of the cochlea, and a small 0.6-mm-diameter hole was manually drilled near the base. An external reservoir was connected to the basal hole with a plastic tube and was used to continuously perfuse oxygenated culture medium through the scala tympani. Acoustic stimuli were delivered to the middle ear with a calibrated loudspeaker connected to the chamber with a plastic tube. In the preparation, the middle ear ossicles were left intact; however, because the entire middle ear was immersed in fluid, the effective SPL was attenuated by 20–30 dB (70). SPLs cited throughout this paper have been corrected for this attenuation.

Method Details.

Confocal imaging. Samples were imaged with a laser scanning confocal microscope (Zeiss LSM 780) controlled with Zen 2012 black edition software (Zeiss). Ca^{2+} imaging with Asante Calcium Red and hair bundle displacements were measured with a 40× water immersion, 0.80-N.A. objective lens (Zeiss Achroplan); FCS measurements were taken with a 60×, 1.0-N.A. water immersion objective (Nikon NIR APO). All images were processed in custom scripts written in MATLAB (The MathWorks).

Electrophysiological recordings. Glass capillaries with a 1.5-mm outer diameter were pulled with a standard electrode puller, filled with artificial endolymph [1.3 mM NaCl, 31 mM $KHCO_3$, 128.3 mM KCl, and 0.023 mM $CaCl_2$ (pH 7.4), with an osmolality of 300 mOs/kg with sucrose] and beveled at 20° to a final resistance of 3–7 MΩ as measured in the culture medium. Fluorescent dyes and other reagents were added to the electrodes as described below. The electrodes were mounted in a manual manipulator and positioned through the apical window close to Reissner's membrane. The final penetration of Reissner's membrane was accomplished with a hydraulic stepping motor. An Ag/AgCl pellet in the culture medium, contiguous with the scala tympani, served as the ground electrode. Just before, and while passing the glass electrode through Reissner's membrane, a linear stimulus isolator (A395 World Precision Instruments) was used to send positive steady-state currents of up to +10 μA. This drives the dyes out of the electrode, while preventing membrane clumps from forming inside the electrode. The average endocochlear potential upon penetration of Reissner's membrane was +25 mV, and a separate set of experiments revealed that it declined at a rate of 9 mV per hour. Microphonic potentials were measured with an Ix1 amplifier (Dagan Instruments) and digitized with a 24-bit A/D board (NI USB-4431; National Instruments) at 10 kHz. Tuning curves were recorded in response to a series of single-tone stimuli at an SPL of 64 dB (decibels relative to 20 μPa) from 60 to 820 Hz, a range that covers the apical region of the guinea pig cochlea, and the peaks were extracted from the digital signals by Fourier analysis. Immediately after dissecting and mounting the preparations, the microphonic potentials were frequently unstable. Tuning curve measurements were repeated every 5 min until the recordings stabilized, and we then proceeded with other measurements. Microelectrodes were used to deliver fluorescent dyes, either iontophoretically or with a brief pressure injection as described below.

Calibration of Ca^{2+}-sensitive dyes. We prepared a series of artificial endolymph-like solutions in which the [Ca^{2+}] was varied from 0 to 1 mM. For a [Ca^{2+}] greater than 10 μM, we prepared a zero-Ca^{2+} endolymph (1.3 mM NaCl, 31 mM $KHCO_3$, and 128.3 mM KCl) and added concentrated $CaCl_2$ stock. For a [Ca^{2+}] less than 10 μM, we prepared two solutions: an artificial endolymph with 1 mM EGTA (1.3 mM NaCl, 31 mM $KHCO_3$, 128.3 mM KCl, and 1 mM EGTA) and a

second solution with 1 mM EGTA and 2 mM $CaCl_2$. All solutions had pH 7.4, and the osmolarities were adjusted with sucrose to 300 mOs/kg. The two solutions were mixed in varying proportions according to the online MaxChelator program (Ca-EGTA Calculator v1.2) to give final free [Ca^{2+}] from 0 to 1 μM (https://somapp.ucdmc.ucdavis.edu/pharmacology/bers/maxchelator/). To each calibration solution, we added 5 μM Asante Calcium Red low-affinity dye (TEFLabs), thoroughly mixed and sonicated the solution, and recorded the fluorescence. Measurements on each standard were repeated five times at 1-min intervals. Fitting the resulting fluorescence ratio to the Hill equation,

$$R = \frac{R_{max} - R_{min}}{1 + (K_d/[Ca^{2+}])^n} + R_{min},$$

where R_{min} and R_{max} are the minimum and maximum fluorescence ratios measured at zero and saturating Ca^{2+} levels, K_d is the dissociation constant, and n is the Hill coefficient, yielded $K_d = 11$ μM and $n = 1$. Using the same procedure (but fitting the raw fluorescence values), the K_d for Oregon Green BAPTA was found to be 37 μM.

Fluorescent staining and imaging. For Asante Calcium Red imaging experiments, concentrated dye stock was diluted to 100 μM in the microelectrode and injected (10 psi for 10 s) into the scala media with a pico-spritzer. During each injection, a time series (approximately one frame per second, 60–100 s in length) was taken to ensure that the injection was successful and that dye did not diffuse into the scala vestibuli. Preparations that had significant dye in the scala vestibuli or for which the dye diffused into the culture medium were discarded. Microphonic potentials were measured before and after, and frequently showed a transient decrease following the pressure injection but typically recovered within 5 min. Confocal images were obtained at 512 × 512 pixels and at a 16-bit pixel depth, with an integration time of 100 μs per pixel and a pinhole of 6.1 Airy units. On some preparations, we recorded Z-stacks with a spacing of 1 μm per slice up to 100 μm in total depth. Fluorescent images were obtained before and after acoustic overstimulation.

Fluorescence correlation spectroscopy. Oregon Green 488 BAPTA-5N (ThermoFisher) was added to the electrode with concentrations ranging from 10 to 100 nM and was ejected with a pressure injection as described above. Because fluorescence correlation spectroscopy necessitates a dye concentration on the order of a few nanomolar units, a concentration too low for standard fluorescence imaging, reflection imaging was used to identify structures in the preparation and identify regions of interest for the measurements. Raw count rates for every position were recorded for 10 s, with each measurement repeated five times and averaged. Autocorrelation functions were computed by the Zen software (Zeiss) and saved for offline analysis. Calibrations indicated an effective detection volume of 3.4 femtoliters, an average endolymphatic dye concentration of 26 nM, and an average dye concentration in the tectorial membrane of 14 nM.

Hair bundle and time-resolved imaging. The cell-permeable dye di-3-aneppdhq (16–32 μM; ThermoFisher) was added in the microelectrode solution and delivered to the hair bundles iontophoretically with positive currents of a few microamperes (5). The preparation was stimulated acoustically near the bundles' best frequency while the microscope recorded a time-locked series of 12 confocal images. Custom software was used to extract pixels acquired at the same phase of the stimulation, which were mapped to 12 images of bundle motion at equally spaced phases of the sine wave, and the resulting trajectories were extracted from the image sequences using an optical flow algorithm as described previously (33). To improve the signal-to-noise ratio, trajectories were obtained for all pixels in a square array, typically 3 × 3, and averaged.

Acoustic overstimulation and EGTA injection. Preparations were exposed to tone bursts at 98 dB SPL, 20 Hz below their best frequency (corresponding to the best frequency at that level), for 10 min. Tone bursts lasted for 700 ms and were repeated at 1-s intervals. Microphonic potentials (at the stimulus frequency) were continuously recorded during the overstimulation. Fluorescent images and frequency sweeps of the microphonic potentials were recorded before the overstimulation, immediately after the overstimulation, and subsequently every 5 min.

For experiments in which multiple solutions were injected into the endolymphatic space after fluorescent staining, the first microelectrode was gently retracted with the hydraulic motor and removed from the apical opening. A second electrode containing endolymph with 100 μM EGTA was inserted at a location close to the opening made by the first electrode. Based on the change in the Ca^{2+} ratio after EGTA injection, the EGTA concentration in the scala media was estimated as 10 ± 4.1 μM ($n = 5$). In some experiments, EGTA injection was followed by injection of endolymph with 1 mM Ca^{2+}. Preparations on which the electrodes were exchanged had robust microphonic potentials after changing the electrodes, demonstrating the intactness of Reissner's membrane.

Quantification and Statistical Analysis. All experiments were repeated multiple times; the number of individual measurements and the number of preparations are discussed in the main text and also in the figure legends. Analyses were performed in MATLAB (R2016b) and in the R environment for statistical computing (71); statistical significance was assessed with repeated-measures analysis of variance, followed by post hoc *t* tests, and by paired *t* tests using Bonferroni corrections in cases where multiple comparisons were performed on the same dataset. Details of the statistical tests used in each case are given in the main text. Areas were measured by drawing a region of interest covering the tectorial membrane, counting the number of pixels, and multiplying with the area of a single pixel. When computing correlations between microphonic potentials and Ca^{2+} changes, the correlation coefficient was determined for each individual preparation and then averaged across preparations. Throughout the main text and in the figure legends results are presented as the mean ± 1 SD.

ACKNOWLEDGMENTS. This work was supported by grants from the Swedish Research Council (Grants 2013-03403 and 2017-06092), the Torsten Söderberg Foundation, the Tysta Skolan Foundation, AFA Försäkrings AB, and the County Council of Östergötland (all to A.F.); Grant DC 00141 from the US National Institute on Deafness and Other Communication Disorders [to Alfred L. Nuttall (CO-PI) and A.F.]; and a fellowship from the Wenner-Gren Foundation (to C.E.S.).

1. Fettiplace R, Kim KX (2014) The physiology of mechanoelectrical transduction channels in hearing. *Physiol Rev* 94:951–986.
2. Corey DP, Hudspeth AJ (1979) Ionic basis of the receptor potential in a vertebrate hair cell. *Nature* 281:675–677.
3. Farris HE, Wells GB, Ricci AJ (2006) Steady-state adaptation of mechanotransduction modulates the resting potential of auditory hair cells, providing an assay for endolymph [Ca^{2+}]. *J Neurosci* 26:12526–12536.
4. Zidanic M, Brownell WE (1990) Fine structure of the intracochlear potential field. I. The silent current. *Biophys J* 57:1253–1268.
5. Jacob S, Pienkowski M, Fridberger A (2011) The endocochlear potential alters cochlear micromechanics. *Biophys J* 100:2586–2594.
6. Johnson SL, Beurg M, Marcotti W, Fettiplace R (2011) Prestin-driven cochlear amplification is not limited by the outer hair cell membrane time constant. *Neuron* 70:1143–1154.
7. Brownell WE, Bader CR, Bertrand D, de Ribaupierre Y (1985) Evoked mechanical responses of isolated cochlear outer hair cells. *Science* 227:194–196.
8. Eatock RA, Corey DP, Hudspeth AJ (1987) Adaptation of mechanoelectrical transduction in hair cells of the bullfrog's sacculus. *J Neurosci* 7:2821–2836.
9. Wu YC, Ricci AJ, Fettiplace R (1999) Two components of transducer adaptation in auditory hair cells. *J Neurophysiol* 82:2171–2181.
10. Holt JR, et al. (2002) A chemical-genetic strategy implicates myosin-1c in adaptation by hair cells. *Cell* 108:371–381.
11. Kros CJ, et al. (2002) Reduced climbing and increased slipping adaptation in cochlear hair cells of mice with Myo7a mutations. *Nat Neurosci* 5:41–47.
12. Pickles JO, Comis SD, Osborne MP (1984) Cross-links between stereocilia in the guinea pig organ of Corti, and their possible relation to sensory transduction. *Hear Res* 15:103–112.
13. Kazmierczak P, et al. (2007) Cadherin 23 and protocadherin 15 interact to form tip-link filaments in sensory hair cells. *Nature* 449:87–91.
14. Howard J, Hudspeth AJ (1987) Mechanical relaxation of the hair bundle mediates adaptation in mechanoelectrical transduction by the bullfrog's saccular hair cell. *Proc Natl Acad Sci USA* 84:3064–3068.
15. Martin P, Mehta AD, Hudspeth AJ (2000) Negative hair-bundle stiffness betrays a mechanism for mechanical amplification by the hair cell. *Proc Natl Acad Sci USA* 97:12026–12031.
16. Kennedy HJ, Crawford AC, Fettiplace R (2005) Force generation by mammalian hair bundles supports a role in cochlear amplification. *Nature* 433:880–883.
17. Hudspeth AJ (2008) Making an effort to listen: Mechanical amplification in the ear. *Neuron* 59:530–545.
18. Peng AW, Effertz T, Ricci AJ (2013) Adaptation of mammalian auditory hair cell mechanotransduction is independent of calcium entry. *Neuron* 80:960–972.
19. Corns LF, Johnson SL, Kros CJ, Marcotti W (2014) Calcium entry into stereocilia drives adaptation of the mechanoelectrical transducer current of mammalian cochlear hair cells. *Proc Natl Acad Sci USA* 111:14918–14923.
20. Bosher SK, Warren RL (1978) Very low calcium content of cochlear endolymph, an extracellular fluid. *Nature* 273:377–378.
21. Wood JD, Muchinsky SJ, Filoteo AG, Penniston JT, Tempel BL (2004) Low endolymph calcium concentrations in deafwaddler2J mice suggest that PMCA2 contributes to endolymph calcium maintenance. *J Assoc Res Otolaryngol* 5:99–110.
22. Salt AN, Inamura N, Thalmann R, Vora A (1989) Calcium gradients in inner ear endolymph. *Am J Otolaryngol* 10:371–375.
23. Ikeda K, Kusakari J, Takasaka T (1988) Ionic changes in cochlear endolymph of the guinea pig induced by acoustic injury. *Hear Res* 32:103–110.
24. Vélez-Ortega AC, Freeman MJ, Indzhykulian AA, Grossheim JM, Frolenkov GI (2017) Mechanotransduction current is essential for stability of the transducing stereocilia in mammalian auditory hair cells. *eLife* 6:e24661.

25. Yamoah EN, et al. (1998) Plasma membrane Ca2+-ATPase extrudes Ca^{2+} from hair cell stereocilia. *J Neurosci* 18:610–624.
26. Warren RL, et al. (2016) Minimal basilar membrane motion in low-frequency hearing. *Proc Natl Acad Sci USA* 113:E4304–E4310.
27. Hyrc KL, et al. (2013) Synthesis and properties of Asante Calcium Red–A novel family of long excitation wavelength calcium indicators. *Cell Calcium* 54:320–333.
28. Takahashi A, Camacho P, Lechleiter JD, Herman B (1999) Measurement of intracellular calcium. *Physiol Rev* 79:1089–1125.
29. Rigler R, Mets Ü, Widengren J, Kask P (1993) Fluorescence correlation spectroscopy with high count rate and low background: Analysis of translational diffusion. *Eur Biophys J* 22:169–175.
30. Kim SA, Heinze KG, Schwille P (2007) Fluorescence correlation spectroscopy in living cells. *Nat Methods* 4:963–973.
31. Banks DS, Fradin C (2005) Anomalous diffusion of proteins due to molecular crowding. *Biophys J* 89:2960–2971.
32. Kurabi A, Keithley EM, Housley GD, Ryan AF, Wong AC (2017) Cellular mechanisms of noise-induced hearing loss. *Hear Res* 349:129–137.
33. Jacob S, Tomo I, Fridberger A, de Monvel JB, Ulfendahl M (2007) Rapid confocal imaging for measuring sound-induced motion of the hearing organ in the apical region. *J Biomed Opt* 12:021005.
34. Kronester-Frei A (1979) The effect of changes in endolymphatic ion concentrations on the tectorial membrane. *Hear Res* 1:81–94.
35. Shah DM, Freeman DM, Weiss TF (1995) The osmotic response of the isolated, unfixed mouse tectorial membrane to isosmotic solutions: Effect of Na+, K+, and Ca^{2+} concentration. *Hear Res* 87:187–207.
36. Freeman DM, Masaki K, McAllister AR, Wei JL, Weiss TF (2003) Static material properties of the tectorial membrane: A summary. *Hear Res* 180:11–27.
37. Verpy E, et al. (2011) Stereocilin connects outer hair cell stereocilia to one another and to the tectorial membrane. *J Comp Neurol* 519:194–210.
38. Hakizimana P, Brownell WE, Jacob S, Fridberger A (2012) Sound-induced length changes in outer hair cell stereocilia. *Nat Commun* 3:1094.
39. Hakizimana P, Fridberger A (2015) Effects of salicylate on sound-evoked outer hair cell stereocilia deflections. *Pflugers Arch* 467:2021–2029.
40. Assad JA, Shepherd GM, Corey DP (1991) Tip-link integrity and mechanical transduction in vertebrate hair cells. *Neuron* 7:985–994.
41. Zhao Y, Yamoah EN, Gillespie PG (1996) Regeneration of broken tip links and restoration of mechanical transduction in hair cells. *Proc Natl Acad Sci USA* 93:15469–15474.
42. Indzhykulian AA, et al. (2013) Molecular remodeling of tip links underlies mechanosensory regeneration in auditory hair cells. *PLoS Biol* 11:e1001583.
43. Yamauchi D, et al. (2010) Expression of epithelial calcium transport system in rat cochlea and vestibular labyrinth. *BMC Physiol* 10:1.
44. Takumida M, Ishibashi T, Hamamoto T, Hirakawa K, Anniko M (2009) Age-dependent changes in the expression of klotho protein, TRPV5 and TRPV6 in mouse inner ear. *Acta Otolaryngol* 129:1340–1350.
45. Ficarella R, et al. (2007) A functional study of plasma-membrane calcium-pump isoform 2 mutants causing digenic deafness. *Proc Natl Acad Sci USA* 104:1516–1521.
46. Goodyear RJ, Richardson GP (2018) Structure, function, and development of the tectorial membrane: An extracellular matrix essential for hearing. *Curr Top Dev Biol* 130:217–244.
47. Huang RH, et al. (2008) Assembly of Weibel-Palade body-like tubules from N-terminal domains of von Willebrand factor. *Proc Natl Acad Sci USA* 105:482–487.
48. Legan PK, Rau A, Keen JN, Richardson GP (1997) The mouse tectorins. Modular matrix proteins of the inner ear homologous to components of the sperm-egg adhesion system. *J Biol Chem* 272:8791–8801.
49. Chakravarti S, Tam MF, Chung AE (1990) The basement membrane glycoprotein entactin promotes cell attachment and binds calcium ions. *J Biol Chem* 265:10597–10603.
50. Bokhove M, et al. (2016) A structured interdomain linker directs self-polymerization of human uromodulin. *Proc Natl Acad Sci USA* 113:1552–1557.
51. Ghaffari R, Page SL, Farrahi S, Sellon JB, Freeman DM (2013) Electrokinetic properties of the mammalian tectorial membrane. *Proc Natl Acad Sci USA* 110:4279–4284.
52. Corns LF, Johnson SL, Kros CJ, Marcotti W (2016) Tmc1 point mutation affects Ca^{2+} sensitivity and block by dihydrostreptomycin of the mechanoelectrical transducer current of mouse outer hair cells. *J Neurosci* 36:336–349.
53. Dallos P (1985) Response characteristics of mammalian cochlear hair cells. *J Neurosci* 5: 1591–1608.
54. Legan PK, et al. (2000) A targeted deletion in alpha-tectorin reveals that the tectorial membrane is required for the gain and timing of cochlear feedback. *Neuron* 28: 273–285.
55. Sirjani DB, Salt AN, Gill RM, Hale SA (2004) The influence of transducer operating point on distortion generation in the cochlea. *J Acoust Soc Am* 115:1219–1229.
56. Fridberger A, Flock A, Ulfendahl M, Flock B (1998) Acoustic overstimulation increases outer hair cell Ca^{2+} concentrations and causes dynamic contractions of the hearing organ. *Proc Natl Acad Sci USA* 95:7127–7132.
57. Jacob S, Johansson C, Fridberger A (2013) Noise-induced alterations in cochlear mechanics, electromotility, and cochlear amplification. *Pflugers Arch* 465:907–917.
58. Housley GD, et al. (2013) ATP-gated ion channels mediate adaptation to elevated sound levels. *Proc Natl Acad Sci USA* 110:7494–7499.
59. Kujawa SG, Liberman MC (2009) Adding insult to injury: Cochlear nerve degeneration after "temporary" noise-induced hearing loss. *J Neurosci* 29:14077–14085.
60. Zwislocki JJ, Kletsky EJ (1979) Tectorial membrane: A possible effect on frequency analysis in the cochlea. *Science* 204:639–641.
61. Gummer AW, Hemmert W, Zenner HP (1996) Resonant tectorial membrane motion in the inner ear: Its crucial role in frequency tuning. *Proc Natl Acad Sci USA* 93:8727–8732.
62. Ulfendahl M, Khanna SM, Heneghan C (1995) Shearing motion in the hearing organ measured by confocal laser heterodyne interferometry. *Neuroreport* 6:1157–1160.
63. Nowotny M, Gummer AW (2006) Nanomechanics of the subtectorial space caused by electromechanics of cochlear outer hair cells. *Proc Natl Acad Sci USA* 103:2120–2125.
64. Fridberger A, Tomo I, Ulfendahl M, Boutet de Monvel J (2006) Imaging hair cell transduction at the speed of sound: Dynamic behavior of mammalian stereocilia. *Proc Natl Acad Sci USA* 103:1918–1923.
65. Ghaffari R, Aranyosi AJ, Freeman DM (2007) Longitudinally propagating traveling waves of the mammalian tectorial membrane. *Proc Natl Acad Sci USA* 104:16510–16515.
66. Legan PK, et al. (2005) A deafness mutation isolates a second role for the tectorial membrane in hearing. *Nat Neurosci* 8:1035–1042.
67. Lukashkin AN, et al. (2012) A mouse model for human deafness DFNB22 reveals that hearing impairment is due to a loss of inner hair cell stimulation. *Proc Natl Acad Sci USA* 109:19351–19356.
68. Russell IJ, et al. (2007) Sharpened cochlear tuning in a mouse with a genetically modified tectorial membrane. *Nat Neurosci* 10:215–223.
69. Legan PK, et al. (2014) Three deaf mice: Mouse models for TECTA-based human hereditary deafness reveal domain-specific structural phenotypes in the tectorial membrane. *Hum Mol Genet* 23:2551–2568.
70. Ulfendahl M, et al. (1996) Mechanical response characteristics of the hearing organ in the low-frequency regions of the cochlea. *J Neurophysiol* 76:3850–3862.
71. R Development Core Team (2016) R: A Language and Environment for Statistical Computing (R Foundation for Statistical Computing, Vienna), Version 3.5.1. Available at www.R-project.org. Accessed June 1, 2018.